

Chemical Reactivity Studies by the Natural-Orbital-Functional 2nd-Order-Møller-Plesset (NOF-MP2) method. Water Dehydrogenation by the Scandium Cation

Jose M. Mercero¹, Jesus M. Ugalde¹ and Mario Piris^{1,2}

¹*Kimika Fakultatea, Euskal Herriko Unibertsitatea (UPV/EHU) and Donostia International Physics Center (DIPC), P.K. 1072, 20080 Donostia, Euskadi, Spain.*

²*Basque Foundation for Science (IKERBASQUE), 48013 Bilbao, Euskadi, Spain.*

The reliability of the recently proposed natural orbital functional supplemented with second-order Møller-Plesset calculations, (NOF-MP2), has been assessed for the mechanistic studies of elementary reactions of transition metal compounds by investigating the dehydrogenation of water by the scandium cation. Both high- and low-spin state potential energy surfaces have been searched thoroughly. Special attention has been paid to the assessment of the capability of the NOF-MP2 method to describe the strong, both static and dynamic, electron correlation effects on the reactivity of Sc^+ (^3D , ^1D) with water. In agreement with experimental observations, our calculations correctly predict that the only exothermic products are the lowest-lying ScO^+ ($^1\Sigma$) and H_2 ($^1\Sigma_g^+$) species. Nevertheless, an in-depth analysis of the reaction paths leading to several additional products was carried out, including the characterization of various minima and several key transition states. Our results have been compared with the highly accurate multiconfigurational supplemented with quasi degenerate perturbation theory, MCQDPT, wavefunction-type calculations, and with the available experimental data. It is observed that NOF-MP2 is able to give a satisfactorily quantitative agreement, with a performance on par with that of the MCQDPT method.

Keywords: NOF-MP2, Transition Metal Cation, Two-State Reactivity, Reactivity

I. INTRODUCTION

Advanced quantum mechanical methods for the determination of the molecular electronic structure have, in the last decade, evolved towards reliable computational algorithms for the elucidation of the mechanisms of chemical reactions, both in the condensed and in the gas phase [1]. Gas phase studies, in particular, constitute the ideal playground where theory and experiment converge straightforwardly. The strictly molecular nature of both approaches, enables direct comparison of their results free from “environmental” perturbations. The large and increasing number of combined theoretical/experimental chemical reaction mechanistic studies, indisputably shows that the development of reliable and computationally efficient density functional theory (DFT) based methods has contributed greatly to this present status [2].

In this vein, the reactions of transition metal cations with a large variety of substrates, including both first- and second-row hydrides [3–8] and, in particular water [9–13], have been exhaustively studied. Thus, the studies alluded to above have firmly established that the earlier transition metal cations (Sc^+ , Ti^+ , V^+ , Cr^+ and Mn^+) are more reactive than their corresponding oxides, while the opposite is true for the late transition metal cations (Co^+ , Ni^+ and Cu^+).

The earlier transition metal cations have high-spin ground states, while the ground states of their corresponding oxide cations are low-spin. For late transition

metals the opposite is found, namely, the metal cations have low-spin ground states and their corresponding oxides have high-spin ground states. This precludes complex reaction mechanisms for which allowance for spin-crossings to occur should be made [14]. Iron, lies in the middle ground, i.e.: Fe^+ and FeO^+ have both high-spin ground states, a fact that does not prevent them from spin-crossings to occur [11].

The distinct gas-phase reactivity of the transition metal cations can naturally be ascribed to the electronic configuration and to the spin state [15] of the reacting metal’s cation. However, the electronic structure of compounds having transition metals are tough for most approximate exchange-correlation functional based DFT methods, for they lack proper consideration of the strong dynamical and static correlation effects arising from the incomplete d -shells of the metals [16]. A fact which forces theoretical analyses to be performed at a higher level of accuracy, involving in many cases multiconfigurational wave-function type methods to properly account for the electron correlation effects. Needless to say that this increases enormously the computational effort and, unfortunately, more often than not it ends up in unbearable computational demands.

Earlier in the 80’s, it was suggested that natural orbital functional theory (NOFT) implementations could be an attractive alternative formalism to current wave-function based algorithms. In spite of the fact that computational schemes based on exact functionals [17–19] were found to be too expensive from a computational point of

view, approximate, albeit rigorous, natural orbital functionals (NOFs) have been developed for practical applications. Approximate NOFs have demonstrated [20] to be more accurate than electron density functionals for highly multiconfigurational systems in particular, and to scale more satisfactorily than multiconfigurational wavefunction type methods with respect to the number of basis functions. An extensive account of the formulation and the development of such approximate NOFs can be found elsewhere [21–25].

Recently, an open-source implementation of NOF based methods has been made available to the quantum chemistry community [26]. The associated computer program [DoNOF](#) is designed to solve the energy minimization problem of an approximate NOF, which describes the ground-state of an N -electron system in terms of the natural orbitals (NOs) and their occupation numbers (ONs). The program includes the NOFs developed in the Donostia quantum chemistry group. In this paper, we use the Piris NOF 7 (PNOF7) approximate NOF, which has proven [27, 28] to be an efficient and accurate enough alternative for strongly correlated electrons.

It is worth noting that PNOF7 is able to describe the complete intra-pair, but only the static inter-pair electron correlation. In order to recover the missing inter-pair dynamic electron correlation, a single-reference global method for the electron correlation was introduced [29, 30], taking as a reference the Slater determinant formed with the NOs of an approximate NOF, in our case PNOF7.

Within this approach, denoted as natural orbital functional - second-order Møller-Plesset (NOF-MP2) method, the total energy of an N -electron system can be cast as,

$$E = \tilde{E}_{hf} + E^{corr} = \tilde{E}_{hf} + E^{dyn} + E^{sta} \quad (1)$$

where \tilde{E}_{hf} is the Hartree-Fock (HF) energy obtained with the NOs, the dynamic energy (E^{dyn}) is derived from a modified MP2 perturbation theory, while the non-dynamic energy (E^{sta}) is obtained from the static component of the employed NOF. Actually, the correction E^{dyn} is based on an orbital-invariant formulation of the MP2 energy [31]. It has been observed that NOF-MP2 is able to give a quantitative agreement for dissociation energies, with a performance comparable to that of the accurate CASPT2 method in hydrogen abstraction reactions [32].

In the present paper, we analyze and assess the performance of NOF-MP2 for the description of the $\text{Sc}^+ + \text{H}_2\text{O} \rightarrow \text{ScO}^+ + \text{H}_2$ reaction. This is the first time that NOF based methods have been used for chemical reaction mechanistic studies of transition metal containing compounds.

We address the singlet and triplet spin-states, with the NOFT for multiplets formulation [30]. The results of our NOF-MP2 (over PNOF7 geometries) calculations are compared with the energies obtained by the MC-QDPT/MCSCF(10,17) level of theory (hereafter MC-

QDPT), as implemented in GAMESS-US [33] program package. The TZPV+ basis set, which has been found to give excellent results for transition metal cation reactions with water [10–12], has been used for all the calculations. This basis set is built starting from the TZVP basis developed by Alrichs et. al. [34, 35], complemented by two sets of p [36], one set of d [37] and three uncontracted f functions [38]. The results shown below reconfirm the reliability of this basis set. Frequencies were calculated for all the reported stationary points and ZPVE corrections were applied to the reported energies. The article is organized as follows. In section 2, we briefly lay the foundations of the NOFT. In section 3, we assess the quality of the results obtained, and finally, in section 4 the conclusions are presented.

II. THEORY

The electronic energy of an approximate NOF is given in terms of the NOs $\{\phi_i\}$ and their ONs $\{n_i\}$ as follows

$$E = \sum_i n_i \mathcal{H}_{ii} + \sum_{ijkl} D[n_i, n_j, n_k, n_l] \langle kl|ij \rangle \quad (2)$$

where \mathcal{H}_{ii} denotes the diagonal elements of the one-particle part of the Hamiltonian involving the kinetic energy and the external potential operators, $\langle kl|ij \rangle$ are the matrix elements of the two-particle interaction, and $D[n_i, n_j, n_k, n_l]$ represents the reconstructed two-particle reduced density matrix (2RDM) from the ONs. Restriction of the ONs to the range $0 \leq n_i \leq 1$ represents a necessary and sufficient condition for ensemble N -representability of the one-particle reduced density matrix (1RDM) [39] under the normalization condition $\sum_i n_i = N$.

Our non-relativistic Hamiltonian is free of spin coordinates, hence a state with total spin S is a multiplet, i.e., a mixed quantum state (ensemble) that allows all possible S_z values. This approach differs from the methods routinely used in electronic structure calculations that focus on the high-spin component or break the spin symmetry. Next, we briefly describe how we do the reconstruction of D to achieve PNOF7 for spin-multiplets. A more detailed description can be found in Ref. [30].

We consider N_I single electrons which determine the spin S of the system, and the rest of electrons ($N_{II} = N - N_I$) are spin-paired, so that all spins corresponding to N_{II} electrons provide a zero spin. We focus on the mixed state of highest multiplicity: $2S + 1 = N_I + 1$, $S = N_I/2$. For example, for two single electrons, $N_I = 2$ and $S = 1$, then we have a mixed state $\{|1, -1\rangle, |1, 0\rangle, |1, 1\rangle\}$ which forms a triplet state. In the absence of single electrons ($N_I = 0$), the energy (2) obviously reduces to a NOF that describes singlet states.

For an ensemble of pure states $\{|SM_s\rangle\}$, we note that

$$\langle \hat{S}_z \rangle = \frac{1}{N_I + 1} \sum_{M_s = -N_I/2}^{N_I/2} M_s = 0. \quad (3)$$

Eq. (3) implies that the expected value of \hat{S}_z for the whole ensemble is zero. Consequently, the spin-restricted theory can be adopted even if the total spin of the system is not zero as is the case in the triplet state. We use a single set of orbitals for α and β spins. All the spatial orbitals will be then doubly occupied in the ensemble, so that occupancies for particles with α and β spins are equal: $n_p^\alpha = n_p^\beta = n_p$.

The next step is dividing the orbital space Ω into two subspaces: $\Omega = \Omega_I \oplus \Omega_{II}$. Ω_{II} is composed of $N_{II}/2$ mutually disjoint subspaces Ω_g . Each of which contains one orbital $|g\rangle$ with $g \leq N_{II}/2$, and N_g orbitals $|p\rangle$ with $p > N_{II}/2$, namely,

$$\Omega_g = \{|g\rangle, |p_1\rangle, |p_2\rangle, \dots, |p_{N_g}\rangle\}. \quad (4)$$

Taking into account the spin, the total occupancy for a given subspace Ω_g is 2, which is reflected in the following sum rule:

$$\sum_{p \in \Omega_{II}} n_p = n_g + \sum_{i=1}^{N_g} n_{p_i} = 1, \quad g = 1, 2, \dots, \frac{N_{II}}{2}. \quad (5)$$

In general, N_g may be different for each subspace, but it should be sufficient for the description of each electron pair. In this work, N_g is equal to a fixed number for all subspaces $\Omega_g \in \Omega_{II}$. The maximum possible value of N_g is determined by the basis set used in calculations. In the current work, our calculations indicated that $N_g = 2$ is sufficient to correctly describe the reaction of Sc^+ with water. In fact, we consider only the ONs that do not exceed a certain threshold, e.g. 0.01. Small ONs are known to contribute only to the dynamic correlation that will be accounted for by the MP2 correction to PNOF7. From (5), it follows that

$$2 \sum_{p \in \Omega_{II}} n_p = 2 \sum_{g=1}^{N_{II}/2} \left(n_g + \sum_{i=1}^{N_g} n_{p_i} \right) = N_{II}. \quad (6)$$

Here, the notation $p \in \Omega_{II}$ represents all the indexes of $|p\rangle$ orbitals belonging to Ω_{II} . It is important to recall that orbitals belonging to each subspace Ω_g vary along the optimization process until the most favorable orbital interactions are found. Therefore, orbitals do not remain fixed in the optimization process, they adapt to the problem.

Similarly, Ω_I is composed of N_I mutually disjoint subspaces Ω_g . In contrast to Ω_{II} , each subspace $\Omega_g \in \Omega_I$ contains only one orbital g with $2n_g = 1$. It is worth

noting that each orbital is completely occupied individually, but we do not know whether the electron has α or β spin: $n_g^\alpha = n_g^\beta = n_g = 1/2$. It follows that

$$2 \sum_{p \in \Omega_I} n_p = 2 \sum_{g=N_{II}/2+1}^{N_\Omega} n_g = N_I. \quad (7)$$

In Eq. (7), $N_\Omega = N_{II}/2 + N_I$ denotes the total number of subspaces in Ω . Taking into account Eqs. (6) and (7), the trace of the 1RDM is verified equal to the number of electrons:

$$2 \sum_{p \in \Omega} n_p = 2 \sum_{p \in \Omega_{II}} n_p + 2 \sum_{p \in \Omega_I} n_p = N_{II} + N_I = N. \quad (8)$$

In Fig. 1, we show the splitting into subspaces of the orbital space Ω used in the study of the reaction $\text{Sc}^+ + \text{H}_2\text{O} \rightarrow \text{ScO}^+ + \text{H}_2$. On the right, the division employed for the triplet ($S = 1$, $N_I = 2$) is depicted, where two orbitals make up the subspace Ω_I , whereas fourteen electrons ($N_{II} = 14$) distributed in seven subspaces $\{\Omega_1, \Omega_2, \dots, \Omega_7\}$ make up the subspace Ω_{II} . On the left is the split used for the singlet ($S = 0$, $N_I = 0$), hence sixteen electrons ($N_{II} = 16$) distributed in eight subspaces $\{\Omega_1, \Omega_2, \dots, \Omega_8\}$ compose the subspace Ω_{II} . Note that the value of N_g has been set equal to two in both cases. Also, seven pairs of electrons are kept frozen in the innermost orbitals and are not shown in the figure.

The construction [24, 40] of an N-representable functional given by Eq. (2) is related to the N-representability problem of D [41]. Using its ensemble N-representability conditions to generate a reconstruction functional leads to PNOF7 [29, 30, 42]. Assuming real spatial orbitals, we obtain

$$E^{PNOF7} = \sum_{g=1}^{N_{II}/2} E_g + \sum_{g=N_{II}/2+1}^{N_\Omega} \mathcal{H}_{gg} + \sum_{f \neq g}^{N_\Omega} E_{fg} \quad (9)$$

where

$$E_g = 2 \sum_{p \in \Omega_g} n_p \mathcal{H}_{pp} + \sum_{q, p \in \Omega_g} \Pi_{qp} \mathcal{K}_{pq}, \quad \Omega_g \in \Omega_{II} \quad (10)$$

with

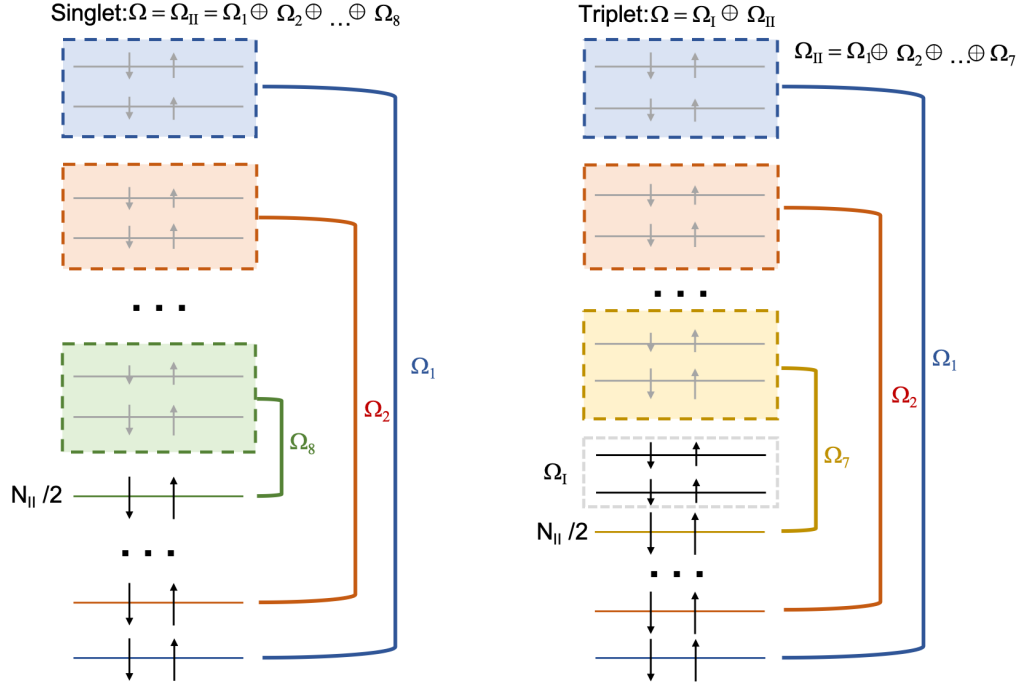
$$\Pi_{pq} = \begin{cases} \sqrt{n_p n_q} & p = q \text{ or } p, q > \frac{N_{II}}{2} \\ -\sqrt{n_p n_q} & p = g \text{ or } q = g \end{cases} \quad (11)$$

is the energy of a pair of electrons with opposite spins. Eq. (10) reduces to the NOF obtained from a ground-state singlet wavefunction, so E_g describes accurately two-electron systems [24]. \mathcal{K}_{pq} are the exchange integrals $\langle pq|qp\rangle$.

In the the last term of Eq. (9), E_{fg} correlates the motion of electrons with parallel and opposite spins belonging to different subspaces ($\Omega_f \neq \Omega_g$):

$$E_{fg} = \sum_{p \in \Omega_f} \sum_{q \in \Omega_g} [n_q n_p (2\mathcal{J}_{pq} - \mathcal{K}_{pq}) - \Phi_q \Phi_p \mathcal{K}_{pq}] \quad (12)$$

Figure 1: Splitting of the orbital space Ω into subspaces used in the study of the reaction $Sc^+ + H_2O \rightarrow ScO^+ + H_2$. The arrows depict the values of the ensemble occupation numbers, alpha (\downarrow) or beta (\uparrow), in each orbital. The seven innermost orbitals with frozen electrons are not shown.



In Eq. (12), \mathcal{J}_{pq} are the usual Coulomb integrals $\langle pq|pq\rangle$, whereas $\Phi_p = \sqrt{n_p(1-n_p)}$. It is not difficult to verify [30] that the PNOF7 reconstruction leads to $\langle \hat{S}^2 \rangle = S(S+1)$ with $S = N_I/2$. Therefore, the PNOF7 results should be exempt from spin contamination effects.

Being an electron-pair-based functional [25], PNOF7 is not capable of recovering the entire dynamic correlation, so we must resort to perturbative corrections if we want to obtain significant total energies. PNOF7 provides the NOs to form the reference energy \tilde{E}_{hf} in Eq. (1), namely,

$$\tilde{E}_{hf} = 2 \sum_{g=1}^{N_\Omega} \mathcal{H}_{gg} + \sum_{f,g=1}^{N_\Omega} (2\mathcal{J}_{fg} - \mathcal{K}_{fg}) - \sum_{g=\frac{N_{II}+1}{2}}^{N_\Omega} \frac{\mathcal{J}_{gg}}{4} \quad (13)$$

In Eq. (13), the last term eliminates the $\alpha\beta$ -contribution to the energy of the singly occupied orbitals since in each pure state $|SM_s\rangle$ of the ensemble there is no such interaction. In this sense, the zeroth-order Hamiltonian for the modified MP2 is constructed from a closed-shell-like Fock operator that contains a HF density matrix with doubly ($2n_g = 2$) and singly ($2n_g = 1$) occupied orbitals.

E^{sta} is the sum of the static intra-space and inter-space

correlation energies:

$$E^{sta} = \sum_{g=1}^{N_{II}/2} \sum_{q \neq p} \sqrt{\Lambda_q \Lambda_p} \Pi_{qp} \mathcal{K}_{pq} - 4 \sum_{f \neq g}^{N_\Omega} \sum_{p \in \Omega_f} \sum_{q \in \Omega_g} \Phi_q^2 \Phi_p^2 \mathcal{K}_{pq} \quad (14)$$

where $\Lambda_p = 1 - |1 - 2n_p|$ is the amount of intra-space static correlation in each orbital as a function of its occupancy. Note that Λ_p goes from zero for empty or fully occupied orbitals to one if the orbital is half occupied.

E^{dyn} is obtained from the second-order correction $E^{(2)}$ of the MP2 method. The first-order wavefunction is a linear combination of all doubly excited configurations, considering one electron with α or β spin in Ω_I . The dynamic energy correction takes the form

$$E^{dyn} = \sum_{g,f=1}^{N_\Omega} \sum_{p,q > N_\Omega}^{N_B} A_g A_f \langle gf|pq\rangle [2T_{pq}^{gf} - T_{pq}^{fg}] \quad (15)$$

where

$$A_g = \begin{cases} 1, & 1 \leq g \leq N_{II}/2 \\ \frac{1}{2}, & N_{II}/2 < g \leq N_\Omega \end{cases} \quad (16)$$

and N_B is the number of basis functions. The amplitudes T_{pq}^{fg} are obtained by solving the modified equations for the MP2 residuals [31]. In order to avoid double counting of the electron correlation, the amount of dynamic

correlation in each orbital p is defined by functions C_p of its occupancy, namely,

$$C_p^{tra} = \begin{cases} 1 - 4(1 - n_p)^2, & p \leq N_\Omega \\ 1 - 4n_p^2, & p > N_\Omega \end{cases} \quad (17)$$

$$C_p^{ter} = \begin{cases} 1, & p \leq N_\Omega \\ 1 - 4(1 - n_p)n_p, & p > N_\Omega \end{cases}$$

where C_p is divided into intra-space (C_p^{tra}) and inter-space (C_p^{ter}) contributions. According to Eq. (17), fully occupied and empty orbitals yield a maximal contribution to dynamic correlation, whereas orbitals with half occupancies contribute nothing. It is worth noting that C_p^{ter} is not considered if the orbital is below N_Ω . Using these functions as the case may be (intra-space or inter-space), the modified off-diagonal elements of the Fock matrix ($\tilde{\mathcal{F}}$) are defined as

$$\tilde{\mathcal{F}}_{pq} = \begin{cases} C_p^{tra} C_q^{tra} \mathcal{F}_{pq}, & p, q \in \Omega_g \\ C_p^{ter} C_q^{ter} \mathcal{F}_{pq}, & otherwise \end{cases} \quad (18)$$

as well as modified two-electron integrals:

$$\langle pq | \widetilde{rt} \rangle = \begin{cases} C_p^{tra} C_q^{tra} C_r^{tra} C_t^{tra} \langle pq | rt \rangle, & p, q, r, t \in \Omega_g \\ C_p^{ter} C_q^{ter} C_r^{ter} C_t^{ter} \langle pq | rt \rangle, & otherwise \end{cases} \quad (19)$$

where the subspace index $g = 1, \dots, N_\Omega$. This leads to the following linear equation for the modified MP2 residuals:

$$\langle ab | \widetilde{ij} \rangle + (\mathcal{F}_{aa} + \mathcal{F}_{bb} - \mathcal{F}_{ii} - \mathcal{F}_{jj}) T_{ab}^{ij} + \quad (20)$$

$$\sum_{c \neq a} \tilde{\mathcal{F}}_{ac} T_{cb}^{ij} + \sum_{c \neq b} T_{ac}^{ij} \tilde{\mathcal{F}}_{cb} - \sum_{k \neq i} \tilde{\mathcal{F}}_{ik} T_{ab}^{kj} - \sum_{k \neq j} T_{ab}^{ik} \tilde{\mathcal{F}}_{kj} = 0$$

where i, j, k refer to the strong occupied NOs, and a, b, c to weak occupied ones. It should be noted that diagonal elements of the Fock matrix (\mathcal{F}) are not modified. By solving this linear system of equations the amplitudes T_{pq}^{fg} are obtained, which are inserted into the Eq. (15) to achieve E^{dyn} .

III. RESULTS AND DISCUSSION

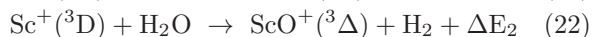
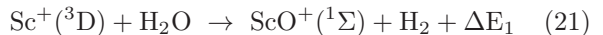
The appropriateness of the selected splitting of the NOs space, Ω , sketched in Fig. 1, is confirmed by the data shown in Table I. The PNOF7-MP2 calculated singlet/triplet splitting energy of the Sc^+ cation compares well with its corresponding experimental mark. It is worth noting that MCQDPT result is very satisfactory, “for the right reason”, and the MP4 one is even better, but, for “the wrong reason”, given the large multiconfigurational character of the electronic structure of both the ground ^3D and the first excited singlet ^1D states of Sc^+ .

Table I: Singlet-Triplet energy splittings, $\Delta_{S/T}$, in eV, for the Sc^+ and for ScO^+ , and dissociation energy, D_0 , in eV, for the $[\text{Sc}(\text{OH})_2]^+$ ion-molecule complex. Zero point vibrational energy corrections have been included.

| | $\Delta_{S/T}^{(\text{Sc}^+)}$ | $\Delta_{S/T}^{(\text{ScO}^+)}$ | D_0 |
|-----------------|--------------------------------|---------------------------------|---------------|
| NOF-MP2 | 0.475 | -3.762 | 1.264 |
| MCQDPT | 0.380 | -3.376 | 1.456 |
| CCSDT/TZVP+[10] | 0.550 | -3.496 | 1.410 |
| B3LYP/TZVP+[10] | 0.916 | -3.292 | 1.580 |
| MCSCF [43] | | -3.450 | 1.571 |
| MP4 [44] | 0.300 | -5.229 | 2.500 |
| Exp. | 0.315[45] | | 1.36±0.13[46] |

The performance of PNOF7-MP2 for the dissociation energy of the $[\text{Sc}(\text{OH})_2]^+$ ion-molecule complex is particularly satisfactory, for it lies within the error-bar range of the experimental mark. Observe that MP4 performs erratically for the prediction of this dissociation energy. For the scandium oxide cation, PNOF7-MP2 predicts a singlet/triplet splitting energy slightly larger than MCQDPT. Having no available experimental results for this species, the similarity of PNOF7-MP2 and MCQDPT values suggest that PNOF7-MP2 should be seen as an accurate estimation. Recall that once again, MP4 does wildly wrong for this particular singlet/triplet splitting energy.

The energetics of the dehydrogenation of water by the Sc^+ cation, reactions (21) and (22), has also been established with a high degree of confidence. The experimental data available for reaction (21), and the highly accurate data available for both reactions, has been collected in Table II.



Armentrout et al. [47], reported in 1984 a value of 1.866 ± 0.304 eV for reaction energy of reaction (21), and ten years later they refined their experimental uncertainty by an order of magnitude, given an experimental estimate of 2.03 ± 0.06 eV [48]. All the calculated reactions energies for reaction (21), shown in Table II, except MP4, lie below the lower bound of the best experimental reaction energy value. However, it is worth noting that PNOF7-MP2 gets the closer of them all, namely, only 6 meV off the mark. The erratic behavior of MP4 calculations for this kind of reactions is manifested here by the calculated overwhelmingly large reaction energy of 4.687 eV. Recall that both B3LYP and CCSD(T) calculations lead to predicted reaction energies in pretty close agreement with both the PNOF7-MP2 and MCQDPT values and the experimental estimate. MCSCF, which lacks an explicit consideration of the dynamical electron correlation effects, yields a reaction energy ~ 0.5 eV lower than methods that treat explicitly dynamical correlation

Table II: ΔE_1 is the energy in eV, including the zero-point vibrational energy corrections, for reaction (21), and ΔE_2 for reaction (22).

| | ΔE_1 | ΔE_2 |
|-----------------|--------------|--------------|
| NOF-MP2 | 1.964 | -1.323 |
| MCQDPT | 1.972 | -1.404 |
| CCSDT/TZVP+[10] | 1.956 | -1.518 |
| B3LYP/TZVP+[10] | 1.939 | -1.253 |
| MCSCF[43] | 1.415 | -2.034 |
| MP4 [44] | 4.687 | |
| Exp.[48] | 2.03±0.06 | |
| Exp.[47] | 1.866±0.304 | |

effects. This emphasizes the fact that the dynamical electron correlation effects must be accounted for, in addition to the static electron correlation effects, in order to yield reliable reaction energies.

The reliability of the optimized geometrical structures of all the intermediates of reactions (21) and (22), is addressed next. The structure of the first intermediate, the encounter ion-molecule complex, $[\text{Sc}(\text{OH}_2)]^+$ (see structure 1C of Fig. 2), has recently been investigated by inspecting the O–H stretching region using infrared laser photodissociation and the method of rare gas atom predissociation. The measured O–H stretches have been found to be shifted to lower frequencies than those for the free water molecule. The significant experimental data, along with our calculated values can be found in Table III.

Table III: OH symmetric and antisymmetric stretching vibrational frequencies, in cm^{-1} , and red shifts (in parentheses) with respect to isolated water vibrational bands for the $[\text{Sc}(\text{OH}_2)]^+$ ion-molecule complex. The experimental values for the ion-molecule complex, which have an argon tag atom bound on the metal cation, have been/ taken from Ref [49]. The reference experimental frequencies for OH_2 have been taken from [50], and the theoretical ones have been calculated at the same level of theory using the harmonic approximation.

| | Exp. | PNOF7 | MCSCF(10,17) |
|----------------------|------------|-----------|--------------|
| ν_{symm} | 3580 (77) | 3730 (61) | 3746 (24) |
| ν_{asymm} | 3656 (100) | 3811 (45) | 3821 (67) |

The experimentally measured frequencies and the red shifts of both, the O–H symmetric and anti-symmetric stretching vibrational bands are nicely predicted by our PNOF7 calculations, as shown in Table III. The discrepancies of the calculated red shifts with respect to their corresponding experimental values, can reasonably be ascribed to the Argon tag-atom attached to the scandium in the experiments, and to the harmonic approximation used in the theoretical calculations. In spite of all this, on the whole, the agreement between theory and experiment is remarkably good.

The electronic structure of the $[\text{Sc}(\text{OH}_2)]^+$ ion-molecule complex deserves a further comment. Indeed, as revealed by the inspection of the ONs of both the MCSCF and the PNOF7 calculations, shown the Table IV, its singlet state corresponds to an almost pure open-shell configuration. The corresponding minimum energy isomer triplet spin state results from a spin-flip, having rather the same ONs, but with a ferromagnetic like coupling of the spins of the two singly occupied NOs. Clearly, both PNOF7 and MCSCF closely agree on this prediction. A feature that can hardly be captured by single-configuration type methods, including most current approximate DFT implementations.

Table IV: Natural occupations numbers of the singlet and triplet spin states of the $[\text{Sc}(\text{OH}_2)]^+$ ion-molecule complex, at the MCSCF and PNOF7 levels of theory. MCSCF orbitals 8–11 belong the fixed occupation inactive core orbitals’ set.

| Orb. # | Singlet 1C | | Triplet 1C | |
|--------|------------|------|------------|------|
| | MCSCF | NOF | MCSCF | NOF |
| 08 | 2.00 | 1.99 | 2.00 | 1.99 |
| 09 | 2.00 | 1.98 | 2.00 | 1.98 |
| 10 | 2.00 | 1.98 | 2.00 | 1.98 |
| 11 | 1.98 | 1.98 | 1.98 | 1.98 |
| 12 | 1.97 | 1.98 | 1.97 | 1.98 |
| 13 | 1.97 | 1.98 | 1.97 | 1.99 |
| 14 | 1.96 | 1.97 | 1.96 | 1.97 |
| 15 | 1.01 | 1.16 | 1.00 | 1.00 |
| 16 | 0.91 | 0.81 | 1.00 | 1.00 |

The singlet and triplet potential energy surfaces for the dehydrogenation of water by Sc^+ has been profusely investigated. Thus, Tilson and Harrison [43] carried an exhaustive MCSCF+1+2 investigation with a relatively small basis set. Later, Ye carried out single reference MP2 like calculations, and finally Irigoras et al. [10], and Russo et al. [51] made a thorough scan of both potential energy surfaces using the hybrid B3LYP exchange-correlation functional complemented with CCSD(T) single point calculations for the refinement of the energies. All these investigations yield the same qualitative picture. Thus, in order to assess the reliability of our PNOF7/TZVP+ optimum intermediates’ structures we shall compare them with the results of MCSCF(10,17) geometry optimization carried out with the TZVP+ basis set. The salient geometrical features of the optimized structures are displayed in Fig. 2.

The optimum PNOF7 and MCSCF geometries for the five intermediates shown in Fig. 2 are very similar. Likewise, they are also similar to the B3LYP optimum geometries reported earlier by Irigoras et al. [10] and Sicilia et al. [51]. The only remarkable difference is that for the triplet-spin potential energy surface the exit channel $\text{ScO}^+ \cdots \text{H}_2$ complex is planar, while the MCSCF favors the H_2 fragment rotated 90 degrees out of the plane with respect to the ScO^+ molecular axis.

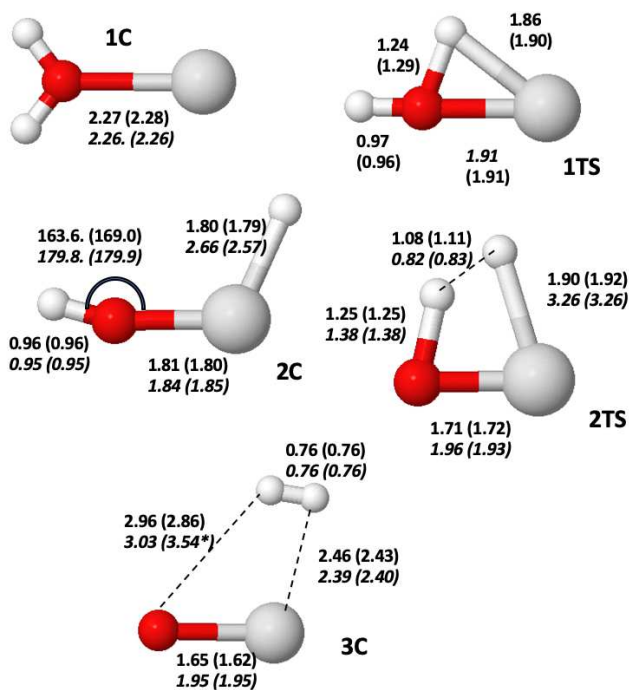


Figure 2: Optimized geometries of intermediate stationary points of the singlet and triplet potential energy surfaces. Plain text values correspond to the singlet optimum geometries; PNOF7 and, MCSCF in parenthesis. Values in italics correspond to their corresponding triplet optimum geometries. The 3C optimum MCSCF geometry, has the H_2 moiety rotated with respect to the PNOF7 geometry. Thus, the MCSCF H–O distance marked with the “*”, turns out to be sizeable larger than its corresponding PNOF7 distance. Images were created with Jmol [52].

Finally, Fig. 3 shows the schematic reaction paths for the $\text{Sc}^+ + \text{OH}_2 \rightarrow \text{ScO}^+ + \text{H}_2$ reaction on the singlet and triplet potential energy surfaces, evaluated at the PNOF7-MP2, B3LYP and MCQDPT levels of theory with the TZVP+ basis set. Although the relative energies of the various intermediates of the proposed mechanism vary slightly among the levels of theory used, the chemistry coming out from the inspection of the three panels of Fig. 3 is the same. Namely, the only exothermic product is $\text{ScO}^+(^1\Sigma) + \text{H}_2(^1\Sigma_g^+)$, which can be reached starting either from the singlet spin reactants, $\text{Sc}^+(^1D) + \text{OH}_2(^1A_1)$, or from the triplet spin state ones, $\text{Sc}^+(^3D) + \text{OH}_2(^1A_1)$, by virtue of the spin crossing occurring in the region between the 1TS and 2C intermediates.

IV. CONCLUSIONS

Current formulations of the natural orbital functional theory based on the Piris ansatz have yield a family of energy functionals of the 1RDM which treat accurately static electron correlation effects, and a substantial portion of the dynamic electron correlation effects [20].

The missing part of the dynamical electron correlation can be brought back in by supplementing the natural orbital functional theory calculations with a perturbational scheme. The implementation of such a scheme into a practical user-friendly code for molecular electronic structure calculations has recently been achieved [26]. This scheme has the advantage to treating electron correlation effects better than current implementations of DFT, and the disadvantage of being more demanding computationally than DFT. Yet its is far less demanding than multiconfigurational theory wave function type implementations. As an example, MCQDPT triplet calculations required around 3 days, 300GB of RAM and more than 20TB of storage, while NOF-MP2 calculations lasted less than 10 hours and required less that 8 GB of RAM.

Herein, we have shown that the recently proposed PNOF7 supplemented with second-order Moller-Plesset calculations, PNOF7-MP2, is very reliable for accurate chemical reaction mechanistic studies of elementary reactions of transition metal compounds, for which strong electron correlation effects are known to be ubiquitous. We have investigated the dehydrogenation of water by the scandium cation and found that (i) the singlet-triplet energy gaps of Sc^+ , and ScO^+ cations are accurately reproduced, (ii) the dissociation energy of the $[\text{Sc}(\text{OH}_2)]^+$ ion-molecule complex is also estimated within the experimental error bars, (iii) the calculated frequencies and red shifts of the OH symmetric and anti-symmetric vibrational bands agree satisfactorily with experimental measurements, (iv) the open-shell electronic structure of the singlet spin state of $[\text{Sc}(\text{OH}_2)]^+$ is also correctly described, along with that of its spin-flip related ground state triplet spin state, (v) the calculated geometries of the intermediate species on both, the singlet and triplet state potential energy surfaces compare satisfactorily with those obtained at the MCSCF level of theory, and (vi) the overall energetics of both potential energy surfaces come in close agreement with those of the highly accurate MCQDPT/MCSCF calculations.

All in all, we believe that PNOF7-MP2 deserves serious consideration as a reliable alternative for chemical reaction mechanistic studies where strong electron correlation effects play a role.

Acknowledgments

The authors thank for technical and human support provided by IZO-SGI SGIker of UPV/EHU and European funding (ERDF and ESF) and DIPC for the generous allocation of computational resources. Financial support comes from the Spanish Office for Scientific Research (MCIU /AEI /FEDER, UE), Ref.:PGC2018-097529-B-100 and Eusko Jaurlaritza (Basque Government), Ref.: IT1254-19.

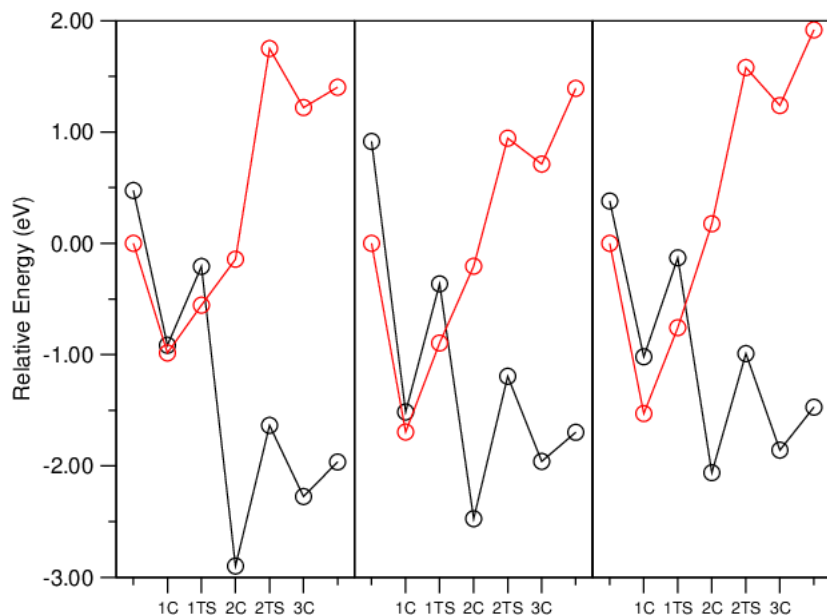


Figure 3: Potential energy surfaces for the triplet spin state (red curves) and for the singlet spin (black curves) state, following the $\text{Sc}^+ + \text{OH}_2 \rightarrow \text{ScO}^+ + \text{H}_2$ reaction path. Left panel: PNOF7-MP2, center panel: B3LYP, right panel: MCQDPT.

- [1] H. Öström, H. Öberg, H. Xin, J. LaRue, M. Beye, M. Dell'Angela, J. Gladh, M. L. Ng, J. A. Sellberg, S. Kaya, et al., *Science* **347**, 978 (2015).
- [2] W. Koch and M. H. Holthausen, *A Chemist's Handbook to Density Functional Theory* (Wiley-VCH, Weinheim, Germany, 2001).
- [3] H. Schwarz, *Angewandte Chemie International Edition* **50**, 10096 (2011).
- [4] A. Bozovic, S. Feil, G. K. Koyanagi, A. A. Viggiano, X. Zhang, M. Schlangen, H. Schwarz, and D. K. Bohme, *Chemistry - A European Journal* **16**, 11605 (2010).
- [5] O. Mo, M. Yanez, J.-Y. Salpin, and J. Tortajada, *Mass Spectrometry Reviews* **26**, 474 (2007).
- [6] O. Lakuntza, J. M. Matxain, and J. M. Ugalde, *ChemPhysChem* **11**, 3172 (2010).
- [7] R. Kretschmer, M. Schlangen, and H. Schwarz, *Chemistry - A European Journal* **18**, 40 (2012).
- [8] O. Lakuntza, J. M. Matxain, F. Ruipérez, J. M. Ugalde, and P. B. Armentrout, *Chemistry - A European Journal* **19**, 8832 (2013).
- [9] D. E. Clemmer, N. Aristov, and P. B. Armentrout, *The Journal of Physical Chemistry* **97**, 544 (1993).
- [10] A. Irigoras, J. E. Fowler, and J. Ugalde, *J. Am. Chem. Soc.* **121**, 574 (1999).
- [11] A. Irigoras, J. E. Fowler, and J. M. Ugalde, *Journal of the American Chemical Society* **121**, 8549 (1999).
- [12] A. Irigoras, O. Elizalde, J. E. Fowler, and J. M. Ugalde, *Journal of the American Chemical Society* **121**, 114 (2000).
- [13] S. Chiodo, O. Kondakova, M. d. C. Michelini, N. Russo, E. Sicilia, A. Irigoras, and J. M. Ugalde, *The Journal of Physical Chemistry A* **108**, 1069 (2004).
- [14] S. Shaik, *Israel Journal of Chemistry* **60**, 938 (2020).
- [15] P. B. Armentrout, *Science* **251**, 175 (1991).
- [16] J. M. Mercero, J. M. Matxain, X. Lopez, D. M. York, A. Largo, L. A. Eriksson, and J. M. Ugalde, *International Journal of Mass Spectrometry* **240**, 37 (2005).
- [17] T. L. Gilbert, *Phys. Rev. B* **12**, 2111 (1975).
- [18] M. Levy, *Proc. Natl. Acad. Sci. USA* **76**, 6062 (1979).
- [19] S. M. Valone, *J. Chem. Phys.* **73**, 1344 (1980).
- [20] I. Mitxelena, M. Piris, and J. M. Ugalde, in *State Art Mol. Electron. Struct. Comput. Correl. Methods, Basis Sets More*, edited by P. Hoggan and U. Ancarani (Academic Press, 2019), *Advances in Quantum Chemistry*, chap. 7, pp. 155–177.
- [21] M. Piris, in *Reduced-Density-Matrix Mechanics: with applications to many-electron atoms and molecules*, edited by D. A. Mazziotti (John Wiley and Sons, Hoboken, New Jersey, USA, 2007), chap. 14, pp. 387–427.
- [22] M. Piris and J. M. Ugalde, *Int. J. Quantum Chem.* **114**, 1169 (2014).
- [23] K. Pernal and K. J. H. Giesbertz, *Top Curr Chem* **368**, 125 (2016).
- [24] M. Piris, in *Many-body approaches at different scales: a tribute to N. H. March on the occasion of his 90th birthday*, edited by G. G. N. Angilella and C. Amovilli (Springer, New York, 2018), chap. 22, pp. 283–300.
- [25] M. Piris, in *Theoretical and Quantum Chemistry at the Dawn of the 21st Century*, edited by T. Chakraborty and R. Carbo-Dorca (Apple Academic Press, New Jersey, USA, 2018), chap. 22, pp. 593–620.
- [26] M. Piris and I. Mitxelena, *Comp. Phys. Comm.* **259**, 107651 (2021).
- [27] I. Mitxelena and M. Piris, *J. Phys. Condens. Matter* **32**, 17LT01 (2020).
- [28] I. Mitxelena and M. Piris, *J. Chem. Phys.* **152**, 064108 (2020).
- [29] M. Piris, *Phys. Rev. Lett.* **119**, 063002 (2017).

- [30] M. Piris, Phys. Rev. A **100**, 032508 (2019).
- [31] M. Piris, Phys. Rev. A **98**, 022504 (2018).
- [32] X. Lopez and M. Piris, Theor. Chem. Acc. **138**, 89 (2019).
- [33] G. M. J. Barca, C. Bertoni, L. Carrington, D. Datta, N. De Silva, J. E. Deustua, D. G. Fedorov, J. R. Gour, A. O. Gunina, E. Guidez, et al., The Journal of Chemical Physics **152**, 154102 (2020).
- [34] A. Schafer, C. Huber, and R. Alrichs, J. Chem. Phys. **97**, 2571 (1992).
- [35] A. Schafer, C. Huber, and R. Alrichs, J. Chem. Phys. **100**, 5829 (1994).
- [36] P. J. Hay, J. Chem. Phys. **66**, 4377 (1977).
- [37] A. J. H. Watchers, J. Chem. Phys. **52**, 1033 (1970).
- [38] K. Raghavachari and G. W. Trucks, J. Chem. Phys. **91**, 1062 (1989).
- [39] A. J. Coleman, Rev. Mod. Phys. **35**, 668 (1963).
- [40] M. Piris, J. M. Matxain, X. Lopez, and J. M. Ugalde, J. Chem. Phys. **133**, 111101 (2010).
- [41] D. A. Mazziotti, Phys. Rev. Lett. **108**, 263002 (2012).
- [42] I. Mitxelena, M. Rodríguez-Mayorga, and M. Piris, Eur. Phys. J. B **91**, 109 (2018).
- [43] J. L. Tilson and J. F. Harrison, J. Phys. Chem. **95**, 5097 (1991).
- [44] S. Ye, Theochem **417**, 157 (1997).
- [45] J. Sugar and C. Corliss, J. Phys. Chem. Ref. Data **14**, 1 (1985).
- [46] T. F. Magnera, D. E. David, and J. Michl, Journal of the American Chemical Society **111**, 4100 (1989).
- [47] N. Aristov and P. B. Armentrout, Journal of the American Chemical Society **106**, 4065 (1984).
- [48] Y.-M. Chen, D. E. Clemmer, and A. P. B., J. Phys. Chem. **98**, 11490 (1994).
- [49] P. D. Carnegie, B. Bandyopadhyay, and M. A. Duncan, Journal of Chemical Physics **134** (2011).
- [50] "molecular vibrational frequencies," in *nist chemistry webbook*, edited by p. j. linstrom and w.g. mallard (national institute of standards and technology, gaithersburg, md, 2010), <http://webbook.nist.gov>.
- [51] N. Russo and E. Sicilia, Journal of the American Chemical Society **123**, 2588 (2001).
- [52] *Jmol: an open-source java viewer for chemical structures in 3d.*, <http://www.jmol.org/>.